Thermo-Optical Delay Line for Optical Coherence Tomography

Eduardo Margallo-Balbás[a*], Gregory Pandraud[b], Patrick J. French[a]

[a] Electronic Instrumentation Laboratory, TU Delft, Mekelweg 4, 2628CD, Delft, The Netherlands
[b] Kavli Institute of Nanoscience-HREM, TU Delft, Lorentzweg 1, 2628CJ Delft, The Netherlands

ABSTRACT

Optical Coherence Tomography (OCT) is a powerful medical imaging technology. Its ability to non-invasively probe tissues in depth with high resolution has lead to applications in many fields of medicine, with a large potential for surgical guidance. One of the technological challenges impairing faster adoption of OCT is the relative complexity of the corresponding optical instrumentation, which translates into expensive and bulky setups. In this paper a compact fast-scanning optical delay line based on the thermo-optical effect of silicon is studied. Although this effect has been applied to other optical components, the necessary frequency behaviour together with the relatively large scanning range required are unique to the application. Cycling speeds of over 1kHz and ranges of more than 1mm are needed for video-rate acquisition of relevant tissue volumes. A structure is proposed to meet these specifications. A bulk micro machined freestanding waveguide is connected to the substrate by means of evenly spaced support beams. It is shown by means of the Finite Element Method that the geometrical parameters of the beams modulate the thermal behaviour of the waveguide. A linear trade-off between maximum working frequency and power dissipation for any given waveguide size and required scanning range has been found. Our results show that the proposed implementation of a fast-scanning delay line can match the requirements of Time Domain Optical Coherence Tomography.

Keywords: Optical Coherence Tomography, Scanning Delay Line, Silicon Photonics, Thermo-Optical Effect, Planar Waveguide Technology

1. INTRODUCTION

Optical Coherence Tomography (OCT) is an increasingly popular imaging technique in medicine [1]. Since the first publications in 1990, it has been subject of active research in fields ranging from cardiology [2] to ophthalmology [3], where it has already found commercial application. It has been often compared to B-mode ultrasound, in the sense that it detects the back-reflected intensity of a focused wave, with the difference that it deals with infrared light instead of acoustic vibrations. This technique is able to deliver high-resolution cross-sectional information of the tissue or material microstructure. Image resolutions ranging from <1 to 20µm can be obtained, while line acquisition rates of more than 100 kHz have been reported [4]. OCT relies on the principle of coherence gating, using the limited coherence length of a broadband source, whose bandwidth basically determines the achievable resolution. The sensitivity and dynamic range possible with this technique are excellent, since the detected signal gets amplified in the interferometric mixing process. Sensitivities in excess of 100dB relative to the available power are easily achieved [5].

Because of the extremely high frequency and speed of the electromagnetic waves as compared to ultrasound, direct electronic detection is not possible and an interferometric construction is needed. Three basic set-ups have been reported for OCT, namely Time-Domain, Fourier-Domain OCT and Swept-Source OCT. Although the latter two have some advantages in terms of sensitivity [6] and speed, the required instrumentation seems less suitable for integration using planar waveguide technology. Therefore, in this paper, we only focus on the first.

[*] Further author information: (Send correspondence to E.M.B.)
E.M.B.: E-mail: e.margallo@tudelft.nl, Telephone: +31-15-2786432, Fax: +31-15-2785755
G.P.: E-mail: g.pandraud@tudelft.nl, Telephone: +31-15-2781602, Fax: +31-15-2785755
P.J.F.: E-mail: p.j.french@tudelft.nl, Telephone: +31-15-2784729, Fax: +31-15-2785755

Optomechatronic Micro/Nano Devices and Components III, edited by Lixin Dong, Yoshitada Katagiri,
Eiji Higurashi, Hiroshi Toshiyoshi, Yves-Alain Peter, Proceedings of SPIE Vol. 6717, 671704, (2007)
0277-786X/07/$18 · doi: 10.1117/12.754324

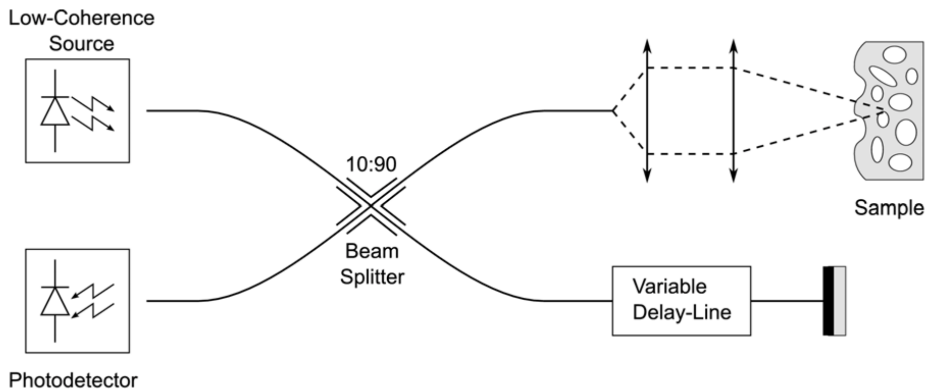

Figure 1. Schematic representation of a Time Domain OCT setup implemented using fibre optics.

Figure 1 illustrates a basic set-up for TD-OCT. This configuration is based on a Twyman-Green interferometer and a low coherence source, e.g., a Super-Luminescent Diode (SLD). A variable temporal delay line is placed in the reference arm, while the sample arm directs light to the tissue under investigation. Scattered light is collected back from the sample and mixed together with the delayed reference. Interference only takes place at the photo-detector if the difference in path-length travelled in both arms falls within the coherence length of the source. In this way, by varying the delay in the reference arm, a depth scan takes place. This is normally accompanied by a lateral displacement of the beam across the sample, generally achieved by means of movable mirrors.

Several embodiments of the scanning delay line have been reported in the literature. The most straightforward one is the galvanometer retroreflector [7]. A simple mirror connected to a linearly scanning galvanometric device is placed in the reference arm. This implementation, with line rates under 10Hz, is too slow for real-time image acquisition and cannot prevent motion artefacts. For these reasons, it has been abandoned but for evaluating fundamental research questions on OCT. Fibre stretching using a piezoelectric transducer [8] has been proposed as a faster replacement of the galvanometer retroreflectors. Typical acquisition rates are around 1000 lines/second, but many practical shortcomings plague this approach. Hystheresis, polarization mismatch, high voltages and high power consumption are examples of the problems that have impeded wider adoption of these devices. The most common solution to date for the delay line in the reference arm is the grating based delay line [9]. This device is based on a transformation of time delay into a linear phase shift in the Fourier domain by means of a grating and a mirror with adjustable tilt. This embodiment typically provides around 2000 lines/second without most of the problems appearing in the previous approach. Disadvantages of the grating based delay lines are mechanical noise, loss of optical power in the grating and chromatic dispersion with broadband sources. Rotating elements [10] have also been introduced in the reference arm to increase the acquisition rates.

OCT systems have been implemented up to now using free-space or fibre optics. Although systems based on fibre optics allow for the most compact, inexpensive and portable instrumentation, the final size and price of the devices are still not adequate for many applications. In fact, we believe that these two technological factors are limiting a faster adoption of OCT in further fields of medicine. It is expected that much more economic and compact devices can be obtained by means of silicon planar waveguide technology. This shift in implementation technology would enable batch production of complete OCT systems with a footprint of few square centimetres. These devices could lead to applications such as OCT-enhanced *smart* pills, but also advance the adoption of OCT as a mainstream surgical guidance technology [11]; a set of applications where cost is a central issue.

In order to realise this concept, a way to produce the different elements in Figure 1 has to be found. Optical couplers and Y-splitters can be obtained in a straightforward manner in planar optical circuits. The integration of III-V semiconductor sources and detectors in the wavelength range of interest (~1.3μm) poses interesting challenges on silicon platforms. This is however a problem that has been widely discussed [12] and is not specific to OCT. For the purposes of this work we will assume that it is possible to couple external sources and detectors to the system and focus on the integration of the fast scanning optical delay line.

In this paper we propose a method to fabricate a variable delay line on-chip by making use of the thermo-optical effect of silicon. This effect consists of a significant modulation of the refractive index of the silicon bulk material by changing its temperature. The thermo-optical coefficient of silicon is relatively large ($\Delta n=1.86\ 10^{-4}\ \Delta T$ at room temperature [13]) and this has been exploited in the design of switches and modulators [14]. The application requirements of OCT are however very different from the ones of devices reported in the literature. Reported designs normally involve changes in path length of few wavelengths, while a large scan range (1-3mm) is typically needed in clinical OCT applications. In the following, we investigate the thermal requirements imposed by the optical constraints and show how they can be achieved. For this, we first propose a parametric bulk micromachined structure with controllable thermal properties. Then, we make use of an iterative optimization procedure based on a thermal Finite Element Method (FEM) simulation to explore the parametric space and find the trade-off condition between the application variables, i.e. power dissipation and device speed. Based on the relationship found, we finally evaluate the adequacy of the proposed device for TD-OCT and compare it with the discussed existing optical-delay line solutions.

2. MATERIALS AND METHODS

2.1. Basic Structure

The thermo-optical effect of silicon can be described at first-order approximation relative to room temperature [13] by equation (1), where Δn corresponds to the change in refractive index and ΔT is the induced temperature change in the silicon in Kelvin degrees. Polarization is not considered at this point as the thermo-optical coefficient is the same for both polarizations [13] and as in the final device only one polarisation will be used.

$$\Delta n = 1.86 \times 10^{-4} \Delta T \qquad (1)$$

The change in path length in the waveguide (Δl) due to this increase in refractive index is given by (2), where l is the total waveguide length exposed to the temperature change, which we assume homogeneous.

$$\Delta l = l \Delta n \qquad (2)$$

It is important to note that (2) assumes that the effective refractive index of the guided mode follows the changes in refractive index of the waveguide core. This is in the case of silicon photonic devices a very good approximation due to the strong confinement of the field within the rib structure.

If we substitute (2) into (1) and extract ΔT, we get the design equation given by (3). This relationship allows us to compute the needed temperature given a required scanning range and device size.

$$\Delta T = \frac{\Delta l}{1.86 \times 10^{-4}\, l} \qquad (3)$$

The required performance goals of the thermo-optical delay line include a round-trip delay difference $2\Delta l$=2mm. Assuming a device length of l=10mm for simplicity, the needed temperature variation between cold and hot states is 537K. Cycling a MEMS structure to this temperature might not be desirable, because of mechanical stress and non-linearity among other potential problems. However, the maximum temperature is inversely proportional to the length of the thermo-optical delay line, so it is always possible to increase the device length so that the maximum temperature remains at a more convenient value. Since these scaling relationships do not affect the relevance of our results, we will keep the 10mm length for simplicity.

It can be observed that the needed temperature is quite significant. In order to keep the dissipated power under control, the thermal resistance to the substrate needs to be modulated to a suitable value. Taking into account the high thermal conductivity of silicon, this means removing most of the material and making the thermally active sections of the waveguide basically freestanding. Figure 2 shows the bulk micro machined structure proposed to this end. The thermal resistance to the substrate is adjusted by means of freestanding silicon support beams, which are also used for mechanical stability and eventually current guiding for the heaters. The support beams were placed alternatively on each side of the freestanding rib waveguide in order to achieve a more homogeneous temperature distribution.

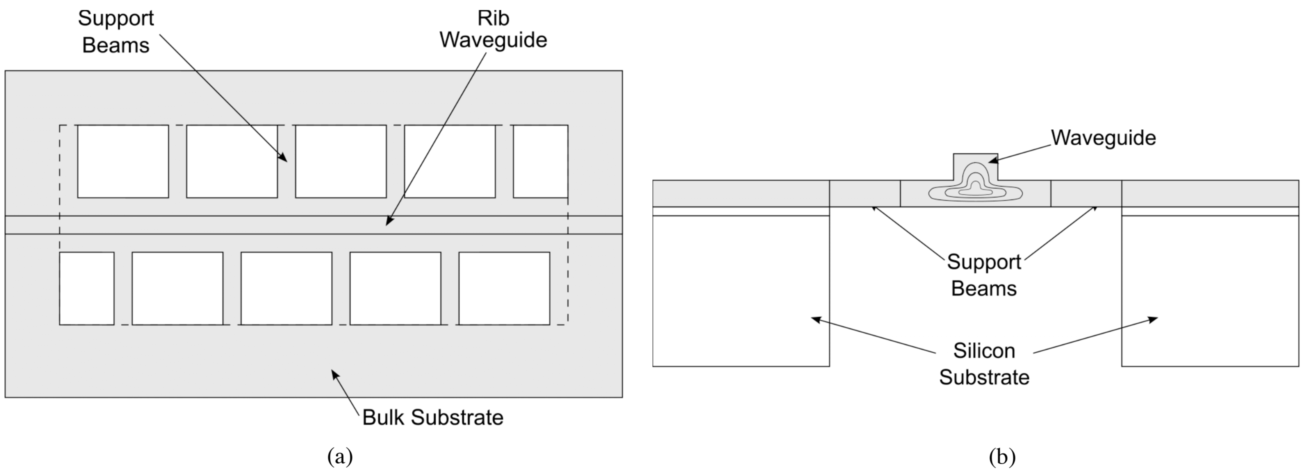

Figure 2. Schematic representation of the studied thermo-optical delay line. a) Top view. b) Front view.

This structural and material choice has several advantages with respect to other possible support configuration with controllable thermal parameters, such as membranes. First, crystalline silicon has an elevated thermal diffusivity (0.8cm^2/s at room temperature) compared to other typical MEMS materials such as oxides and nitrides, which is important for fast operation. Second, the thermal properties of the structure can be readily controlled by means of changing the geometry of the support beams, which can be in turn accurately defined using lithography. Finally, this structure lends itself to simple fabrication using Silicon On Insulator wafers and bulk micromachining.

2.2. FEM Simulations

The behaviour of the structure was explored using the commercial ANSYS Finite Element Environment. Although an analytical approach based on an idealised model could have been used, FEM methods allow for a more flexible problem description. They make the task of considering second order effects such as convection or temperature dependent material properties more manageable. An iterative optimisation algorithm was run with the number of support beams per unit length and their length as the parameters and the time constant of the system as the minimisation goal. Several boundary constraints were introduced in the optimisation loop. First, it was required that the mean steady state temperature along the delay line with active heating be 537°C and that the length of the support beams be shorter than 200μm to prevent structures with too large aspect ratios. Then, a limit of 10% was set between the highest and lowest temperature on the waveguide. Finally, geometrical constraints were added in the form of waveguide and support beam cross-sections. These are mainly limited by the available fabrication technology, as we will see that smaller devices always perform better in the trade-off between power dissipation and device speed.

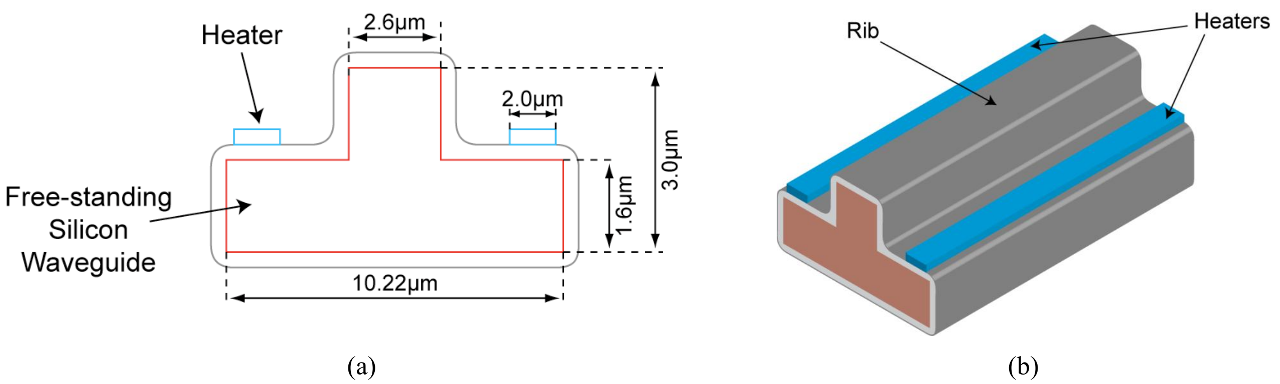

Figure 3. a) Detail of the waveguide cross-section, showing the position of the heaters used in the three dimensional simulation. The dimensions shown correspond to set A. b) Illustration of the symmetrical position of the heaters along the freestanding structure.

Each of the FEM simulations in the loop was conducted using ideal line elements for each of the support elements and for each of the waveguide stages. Line elements were chosen to speed up the simulation, taking the iterative process needed into account. Given the large aspect ratio of the elements in all the devices, the idealization to a line element was expected to be a good approximation, but this was checked using several more realistic simulations based on three-dimensional elements for comparison. In this later case, the translational symmetry of the structure was exploited to reduce the required computational time.

The temperature of the substrate was assumed to stay constant at fixed temperature (0°C) through the heating and cooling cycles. Considering the high thermal conductivity and mass of the bulk silicon substrate compared to the freestanding structure, this is a reasonable assumption with proper device cooling. For the simulations based on line elements, it was accepted that heat was generated homogeneously in the volume of the waveguide. For the three-dimensional calculations, two ideal heaters were defined on each side of the waveguide and heat was generated within them. Convection was taken into account in all simulations. However, it was found that its effect was minor for the structures considered and it can be neglected in most cases.

In order to evaluate the impact of minimum feature size on device performance, we studied three dimension sets. Dimension set A has a waveguide cross-section of 20μm^2 and 2μm^2 for the support beams. Dimension set B has a waveguide cross-section of 4μm^2 and 2μm^2 for the support beams. Finally, dimension set C has a waveguide cross-section of 1 μm^2 and 0.5 μm^2 for the support beams. The exact geometry of the rib waveguide is abstracted in the simulation with line elements and only the cross-sectional area is relevant. In the full three-dimensional computation the exact rib parameters were chosen to fulfil the single-mode waveguide condition (one wave travelling) [15]. For dimensional set A, the values were 2.6μm rib width, 3μm total waveguide height and 1.4μm etch depth. As we will see, given the large aspect ratio of all the elements involved, the exact shape of the wave-guiding region had little impact on the thermal behaviour. Figure 3a illustrates the meaning of these geometrical parameters, producing a total cross-sectional area of 20μm^2.

3. RESULTS

Table 1 summarises the obtained results for different values of dissipated power. L_{el} (μm) is the length of the supporting beams. N_{el} (/mm) is the number of supporting elements per millimetre. The cut-off scanning frequency (f_s) corresponds to twice the -3dB thermal cut-off frequency (f_t), as the scanning range is covered twice per heating cycle. It is traversed once in the heating phase and one more time in the cooling phase. The cut-off scanning frequency (f_s) was the optimised parameter. It is interesting to remark that the maximum working frequencies of all dimension sets keep proportionality relationships equal to the ratio of their waveguide cross-sections. This can be observed easily in Figure 4b, where the logarithmic plot makes the effect of feature size most obvious. No significant analogous effect was found for the dimensional parameter associated with the support beams. For all dimension sets, the required temporal performance is easily achieved, even for the most moderate power levels. The smallest waveguide dimensions (set C), deliver extremely high line rates. Even for the larger waveguides (set A), reasonable scanning speeds are possible within a modest power budget.

Table 1. Cut-off scanning frequency as a function of dissipated power and geometrical parameters for the thermal structure.

$P_0=P_{Peak}/2$ (mW)	$P_0=P_{Peak}/2$ (mW) $f_s=2f_t$ (kHz)			N_{el}(/mm)			L_{el} (μm)		
	A	B	C	A	B	C	A	B	C
100	1.5	7.6	28.2	1.7	1.5	6.7	69.6	20.4	44.8
250	4.4	18.7	76.5	4.6	5.4	14.9	54.7	53.1	39.2
500	8.6	36.9	135.0	8.8	7.3	32.3	53.0	34.8	43.3
1000	16.2	72.4	257.0	21.2	17.2	46.0	64.0	46.5	31.9

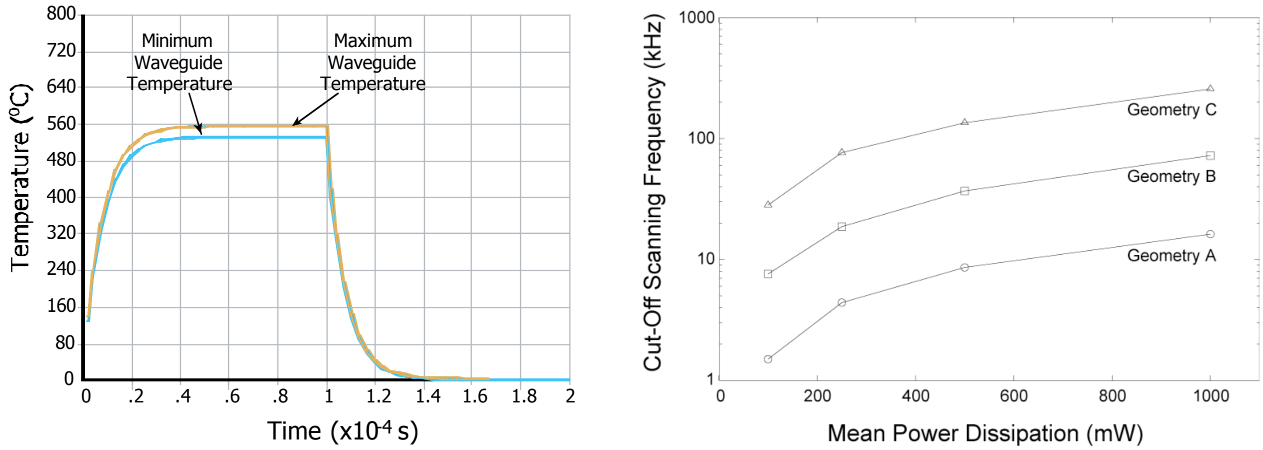

(a) (b)

Figure 4. a) Temporal response to square wave excitation at the maximum and minimum temperature points in the waveguide b) Dependency of the maximum scan rate on the allowed dissipated power during operation

The temporal response under square wave excitation for temperature in the waveguide is depicted in Figure 4a. These simulations correspond to the optimized structure for 1W mean dissipated power and set B of cross-sections. The curves labelled minimum and maximum of temperature correspond to the points closest and farthest to the support beams, respectively. It can be seen that the temperature and therefore the refractive index are relatively homogeneous along the waveguide direction.

Figure 4b depicts the relationship between allowed dissipated power and maximum operational frequency in logarithmic scale. The trade-off between power and speed becomes explicit. Faster operation requires a lower resistance to the substrate for a swift dissipation of heat stored in the waveguide. However, this leads to higher power demands in order to reach the required final temperature. This trade-off between power dissipation and maximum operational frequency is approximately linear in the range of interest, which permits to dimension the structure in a flexible way. However, a slight deviation from this linear relationship takes place with growing available power budgets. This is thought to be due to increased thermal capacitance distributed over the growing number of support beams, which decreases the overall speed of the thermal system.

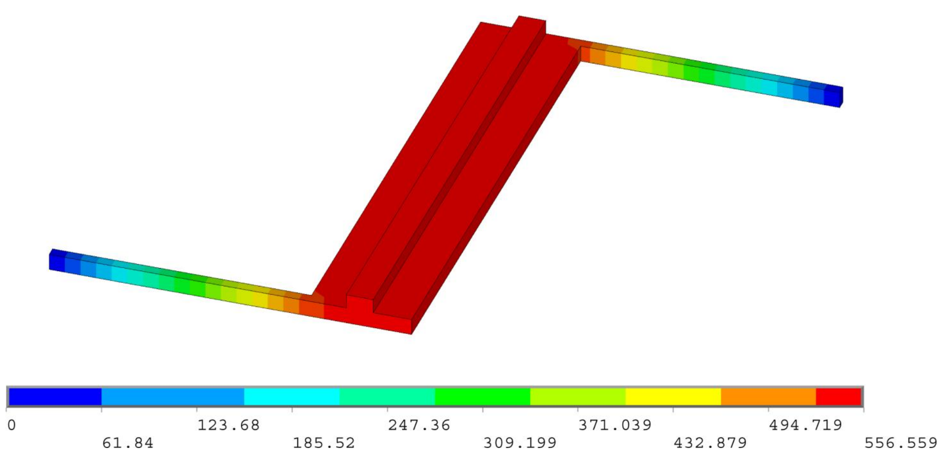

Figure 5. Temperature distribution within a segment of the freestanding waveguide with the dimension set A. Heat generation occurs in two heaters on both sides of the central rib. All values are in Celsius degrees relative to the substrate.

Figure 5 shows a three-dimensional FEM simulation of temperature distribution in a segment of a waveguide at the maximum of the heating cycle. The geometry is consistent with dimensional set A. Heat was introduced by means of two parallel strip heaters placed symmetrically on both sides of the rib, as illustrated in Figure 3b. The translational symmetry of the structure, assumed infinite in the direction of the waveguide has been exploited to reduce the simulation of the whole device to a single segment. It can be observed that temperature distribution is very homogeneous in the rib, even close to the support beams. Although the presented simulation corresponds to the maximum of temperature distribution, heat propagation within the waveguide is very fast and throughout the heating and cooling cycles the relative temperature distribution in the structure is analogous to the depicted one. Considering that the field is strongly confined underneath the rib (see Figure 6), the refractive index modulation will closely follow the imposed thermal cycling. This behaviour is consistent with the findings of the simplified simulation based on line elements. It has been observed that also the temporal behaviour and conclusions drawn from the line element simulations were reproduced in the three-dimensional test simulations with good accuracy.

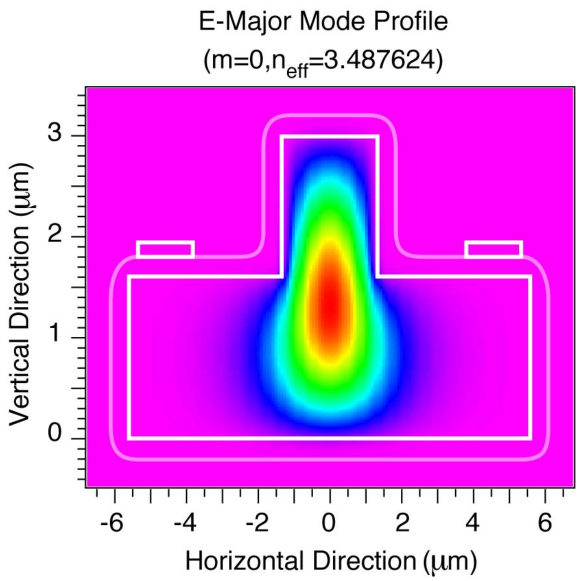

Figure 6. Field distribution within a rib waveguide of dimensional set A for the propagating TE mode, showing the strong confinement of the optical energy under the silicon rib. The geometry has been overlaid in white colour.

4. CONCLUSIONS

We have found that the temporal requirements imposed by OCT on the thermo-optical delay line can be fulfilled using a modest power budget of less than 1W. Compared to other reported delay lines for OCT, the proposed concept has the potential for very high line scan rates, on a pair with the ones achievable with the fastest grating-based delay lines and even with high-end Fourier Domain OCT.

It is in any case important to note that the dimensions of the waveguide have a direct impact on the trade-off between power and operation speed. Smaller waveguides are needed for the fastest depth scans at any given level of power consumption. Silicon rib waveguides with the dimensions discussed in the paper have been reported in the literature [16,17], but their fabrication can be challenging. However, it should be possible to achieve very acceptable line rates even with common micro fabrication facilities. Especially if regions of higher power dissipation are explored, very fast devices can be produced.

Although in this work the devices have been driven with a square wave in order to obtain the thermal time constant of the system, it is important to note that the desired temperature waveform is a perfect triangular wave, so that the optical phase shift changes linearly with time. This leads to an optical intensity that is modulated at a single frequency and makes image acquisition more straightforward. Driving the devices close to the thermal cut-off frequency can easily induce a non-linearity in the temporal phase ramp.

A possible solution to improve the quality of the ramp at high frequencies is to include the thermal filtering effect in the excitation waveform. Usage of metal heaters with well-defined resistance-temperature relationships can allow for a direct determination of the waveguide temperature. This in combination with a feedback loop for heater actuation can in fact achieve the mentioned goal of tuning the excitation waveform to the system response, and increase the frequency range in which the device can be operated. In principle, the reported device could be operated with a duty cycle of 100%.

However, the mentioned non-linearity problems could make it advisable to reduce this duty-cycle for more ideal behaviour, especially for the high end of line acquisition rates.

A shortcoming of this study is the idealisation of the device models used for the simulations, e.g. not taking into account processing imperfections, needed insulation layers between heater and silicon substrate, finite mass of the heaters or limited heat dissipation through the bulk silicon wafer. It is at this point necessary to perform experimental work on real fabricated devices and analyse possible deviations from the simulated values. Furthermore, our focus up to now was merely the thermal behaviour of the structure. However, the interaction between the introduced thermal elements (heaters, support beams) and the optical behaviour needs more careful attention. In particular, a comparable structure in InP demonstrated 0.24dB excess loss per pair of support beams [18], although this value is expected to vary strongly with the exact choice of geometrical parameters for the wave-guiding region.

In this work we have proposed an appropriate structure for the construction of these thermo-optical devices using Silicon On Insulator technology and have demonstrated an iterative method for obtaining the optimum geometrical parameters for any desired combination of power budget and technological possibilities. The thermo-optical effect of silicon appears from our results adequate for the realisation of a fast scanning variable delay line compatible with silicon photonic platforms. This is a step forward towards the realisation of a compact OCT system based on silicon planar waveguide technology. Current research is focused on fabricating the devices and comparing their thermal performance to the simulation results.

ACKNOWLEDGMENTS

The Dutch Technology Foundation STW has supported this research, under contract number STW7505. Financial assistance from the Delft Centre for Mechatronics and Microsystems is gratefully acknowledged. The authors want to thank the DIMES process crew for support with device fabrication.

REFERENCES

1. M. Brezinski, *Optical Coherence Tomography: Principles and applications*, Academic Press, 2006.
2. I.-K. Jang, B.E. Bouma, D.H. Kang, S.-J. Park, S.-W. Park, K.-B. Seung, K.-B. Choi, M. Shishkov, K. Schlendorf, E. Pomerantsev, S.L. Houser, H.T. Aretz, and G.J. Tearney, “Visualization of coronary atherosclerotic plaques in patients using optical coherence tomography: comparison with intravascular ultrasound,” J. Am. Coll. Cardiol., 39, 604-609 (2002)
3. V. Guedes, “Optical coherence tomography measurement of macular and nerve fiber layer thickness in normal and glaucomatous human eyes,” Ophthalmology, 110, 1 (2003)
4. M. W. Jenkins, D. C. Adler, M. Gargesha, R. Huber, F. Rothenberg, J. Belding, M. Watanabe, D. L. Wilson, J. G. Fujimoto, and A. M. Rollins, “Ultrahigh-speed optical coherence tomography imaging and visualization of the embryonic avian heart using a buffered Fourier Domain Mode Locked laser,” Opt. Express 15, 6251-6267 (2007)
5. D. Huang, E.A. Swanson, C.P. Lin, J.S. Schuman, W.G. Stinson, W. Chang, M.R. Hee, T. Flotte, K. Gregory, C.A. Puliafito and J.G. Fujimoto, “Optical coherence tomography,” Science, 254, 5035, 1178-1181 (1991)
6. M. Choma, M. Sarunic, C. Yang, and J. Izatt, "Sensitivity advantage of swept source and Fourier domain optical coherence tomography," Opt. Express 11, 2183-2189 (2003)
7. M. G. Ducros, J. D. Marsack, H. G. Rylander III, S. L. Thomsen, and T. E. Milner, "Primate retina imaging with polarization-sensitive optical coherence tomography," J. Opt. Soc. Am. A 18, 2945-2956 (2001)
8. G. J. Tearney, B. E. Bouma, S. A. Boppart, B. Golubovic, E. A. Swanson, and J. G. Fujimoto, "Rapid acquisition of in vivo biological images by use of optical coherence tomography," Opt. Lett. 21, 1408 (1996)
9. G. J. Tearney, B. E. Bouma, and J. G. Fujimoto, "High-speed phase- and group-delay scanning with a grating-based phase controldelay line," Opt. Lett. 22, 1811-1813 (1997)
10. A. L. Oldenburg, J. J. Reynolds, D. L. Marks, and S. A. Boppart, "Fast-Fourier-Domain Delay Line for in vivo Optical Coherence Tomography with a Polygonal Scanner," Appl. Opt. 42, 4606-4611 (2003)
11. Z. Yaqoob, J. Wu, E.J. McDowell, X. Heng, and C. Yang, “Methods and application areas of endoscopic optical coherence tomography,” J. Biomed. Opt., 11, 6 (2006)
12. J. Brouckaert, G. Roelkens, D. Van Thourhout, and R. Baets, "Thin-Film III–V Photodetectors Integrated on Silicon-on-Insulator Photonic ICs," J. Lightwave Technol. 25, 1053-1060 (2007)
13. Nazarova, N.A., Romanova, G.L. and Yaskov, A.D. “Refractometric Characteristics of Silicon”, Sov. J. Opt. Technol., 55, 220 (1988)

14. Treyz, G. V. “Silicon Mach-Zehnnder Waveguide Interferometers Operating at 1.3µm,” Electron. Lett. 27, 118 (1991)
15. Soref, R. A., Schmidtchen, J. and Petermann, K., J. “Large single-mode rib waveguides in GeSi-Si and Si-on-SiO_2,” Quantum Electron. 27, 1971 (1991)
16. S. Lardenois, D. Pascal, L. Vivien, E. Cassan, S. Laval, R. Orobtchouk, M. Heitzmann, N. Bouzaida, and L. Mollard, "Low-loss submicrometer silicon-on-insulator rib waveguides and corner mirrors," Opt. Lett. 28, 1150-1152 (2003)
17. C. A. Barrios, V. R. Almeida, R. Panepucci, and M. Lipson, "Electrooptic Modulation of Silicon-on-Insulator Submicrometer-Size Waveguide Devices," J. Lightwave Technol. 21, 2332- (2003)
18. D.P. Kelly, M.W. Pruessner, K. Amarnath, M. Datta, S. Kanakaraju, L.C. Calhoun and R. Ghodssi, “Monolithic suspended optical waveguides for InP MEMS”, Phot. Tech. Lett., 16, 5, 1298-1300 (2004)